

YOLO-TS: Real-Time Traffic Sign Detection with Enhanced Accuracy Using Optimized Receptive Fields and Anchor-Free Fusion

Junzhou Chen, Heqiang Huang, Ronghui Zhang, Nengchao Lyu, Yanyong Guo, Hong-Ning Dai, Hong Yan,
Fellow, IEEE

Abstract—Ensuring safety in both autonomous driving and advanced driver-assistance systems (ADAS) depends critically on the efficient deployment of traffic sign recognition technology. While current methods show effectiveness, they often compromise between speed and accuracy. To address this issue, we present a novel real-time and efficient road sign detection network, YOLO-TS. This network significantly improves performance by optimizing the receptive fields of multi-scale feature maps to align more closely with the size distribution of traffic signs in various datasets. Moreover, our innovative feature-fusion strategy, leveraging the flexibility of Anchor-Free methods, allows for multi-scale object detection on a high-resolution feature map abundant in contextual information, achieving remarkable enhancements in both accuracy and speed. To mitigate the adverse effects of the grid pattern caused by dilated convolutions on the detection of smaller objects, we have devised a unique module that not only mitigates this grid effect but also widens the receptive field to encompass an extensive range of spatial contextual information, thus boosting the efficiency of information usage. Evaluation on challenging public datasets, TT100K and CCTSDB2021, demonstrates that YOLO-TS surpasses existing state-of-the-art methods in terms of both accuracy and speed. The code for our method will be available.

Index Terms—Traffic sign recognition, small object detection, YOLO, dilated convolution

I. INTRODUCTION

TRAFFIC signs are crucial components of transportation systems, playing a vital role in enabling drivers and autonomous vehicles to accurately capture road information.

Our manuscript was first submitted to IEEE Transactions on Intelligent Transportation Systems on June 20, 2024.

This project is jointly supported by National Natural Science Foundation of China (Nos. 61003143, 52172350), Guangdong Basic and Applied Research Foundation (Nos. 2021B1515120032, 2022B1515120072), Guangzhou Science and Technology Plan Project (No. 2024B01W0079), Nansha Key RD Program (No. 2022ZD014), Science and Technology Planning Project of Guangdong Province (No. 2023B1212060029). (*Corresponding author: Ronghui Zhang.*)

Junzhou Chen, Heqiang Huang, Ronghui Zhang are with the Guangdong Provincial Key Laboratory of Intelligent Transport System, School of Intelligent Systems Engineering, Sun Yat-sen University, Guangzhou 510275, China. (e-mail: chenjunzhou@mail.sysu.edu.cn; huanghq77@mail2.sysu.edu.cn; zhangrh25@mail.sysu.edu.cn).

Nengchao Lyu is a professor of Intelligent Transportation Systems Research Center, Wuhan University of Technology, Wuhan 430063, China. (e-mail: lnc@whut.edu.cn).

Yanyong Guo is with the School of Transportation, Southeast University, Nanjing 210097, China. (email: guoyanyong@seu.edu.cn).

Hong-Ning Dai is with the Department of Computer Science, Hong Kong Baptist University, Hong Kong. (E-mail: hndai@ieee.org).

Hong Yan is with the Department of Electrical Engineering, City University of Hong Kong, Kowloon, Hong Kong. (email: h.yan@cityu.edu.hk).

As shown in Fig. 1, by accurately identifying traffic signs in driving scenarios, autonomous driving systems can make more intelligent and safer driving decisions based on real-time road conditions. This reduces the occurrence of traffic accidents and ensures the safety of both people and vehicles. With the advancement of deep learning, notably through sophisticated object detection technologies like Faster R-CNN [1] and YOLO [2], the performance of object detectors has significantly improved. Particularly, one-stage detectors have been extensively employed across various domains, including traffic sign [3]–[6], vehicle [7]–[9], and pedestrian detection [10]–[13], due to their efficient balance between accuracy and speed.

Despite these technological advancements, detecting small traffic signs with vehicle-mounted cameras remains a formidable challenge. This difficulty primarily arises from their low resolution and limited informational content. For example, within an image of 2048×2048 pixels, a sign may only span an area of 30×30 pixels. Thus, efficiently detecting such small objects remains one of the significant challenges in the object detection field.

To enhance the performance of small object detection, many studies have focused on creating high-resolution feature maps [14]–[16]. This approach aims to provide richer feature representations for accurate predictions. However, these methods often overlook the importance of aligning the receptive field size with the spatial regions of small objects. Additionally, employing top-down architectures with skip connections to merge low-level and high-level features across different scales has improved detection accuracy [17]–[19]. However, the complexity of these networks raises computational costs during both training and testing, hindering real-time detection. Thus, there is a pressing need for a solution that tackles the challenges of small object detection, high computational demands, and real-time processing.

To address the challenges of accurately detecting small traffic signs, we present YOLO-TS, a novel small object detection framework inspired by the YOLO (You Only Look Once) series models and specifically optimized for traffic sign detection. This framework aims to significantly enhance both the precision and real-time performance of small object detection, and has demonstrated outstanding performance among various object detectors, as shown in Fig. 2. By incorporating advanced techniques and optimization strategies, YOLO-TS ensures robust and efficient detection in various

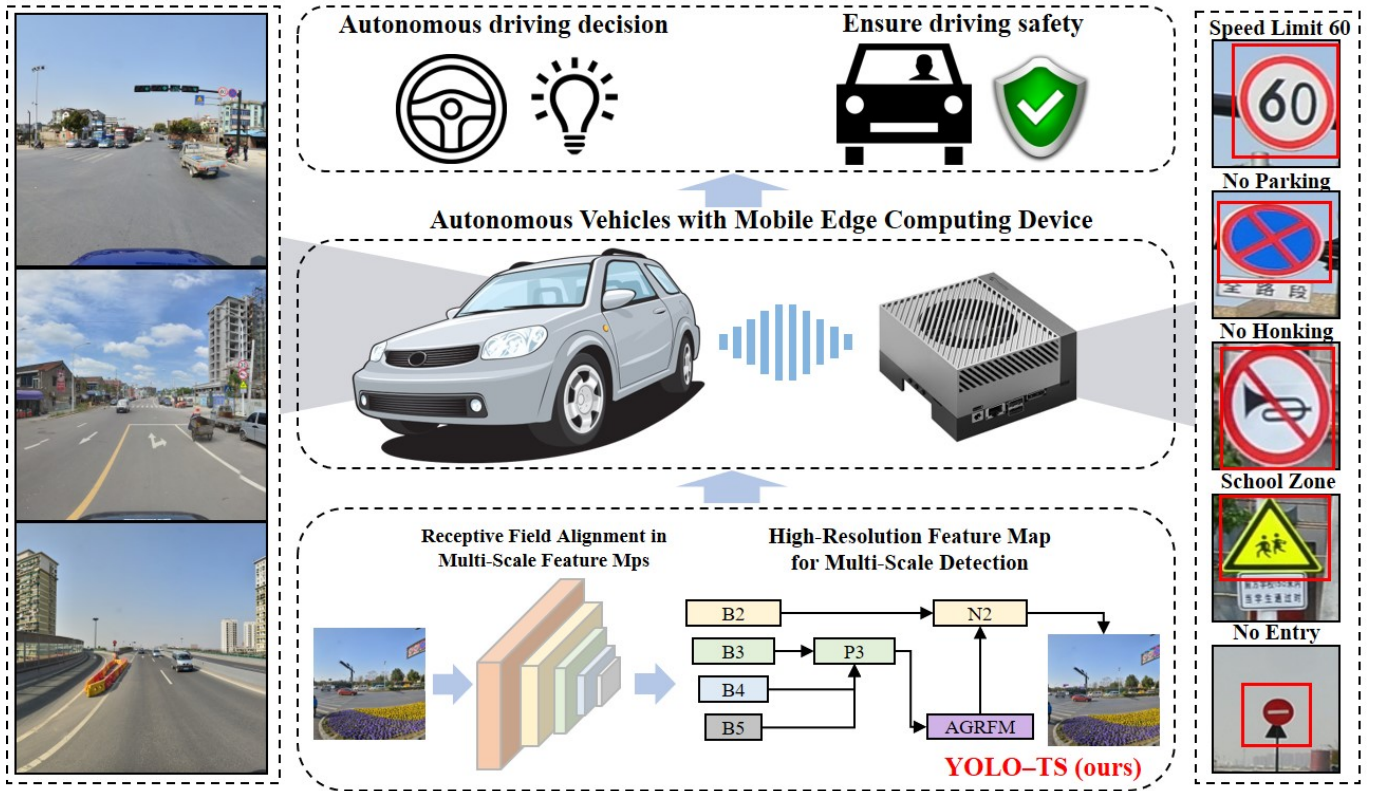


Fig. 1. Application Scenarios of Traffic Sign Detection in Autonomous Driving [20].

driving environments and makes the following contributions to the field of real-time traffic sign detection:

1) **Receptive Field Alignment in Multi-Scale Feature Maps:** We introduce a novel sensory field-matching strategy that aligns the receptive fields of multi-scale feature maps with the size distribution of traffic signs in the dataset. Addressing the challenge of accurately detecting small objects, this alignment enhances detection precision and speed by ensuring that the receptive fields are optimally configured for various traffic sign sizes.

2) **High-Resolution Feature Map for Multi-Scale Detection:** To overcome the limitations of traditional multi-scale detection methods, we develop an innovative approach that leverages high-resolution feature maps enriched with contextual information to predict objects across multiple scales. This strategy enhances the flexibility of the anchor-free method, significantly enhancing both precision and speed, and enabling more robust and efficient traffic sign detection in real-time applications.

3) **Anti-Grid Receptive Field Module (AGRFM):** In response to the grid effect inherent in dilated convolutions, we design the AGRFM. This module integrates regular convolutions with high dilation rates, enhancing the extraction of small object features by maintaining the continuity of feature maps. Consequently, the overall utilization of spatial information is improved, significantly boosting detection accuracy and reliability.

4) **Experiment Validation:** Extensive experiments conducted on the TT100K [21] and CCTSDB2021 [22] datasets

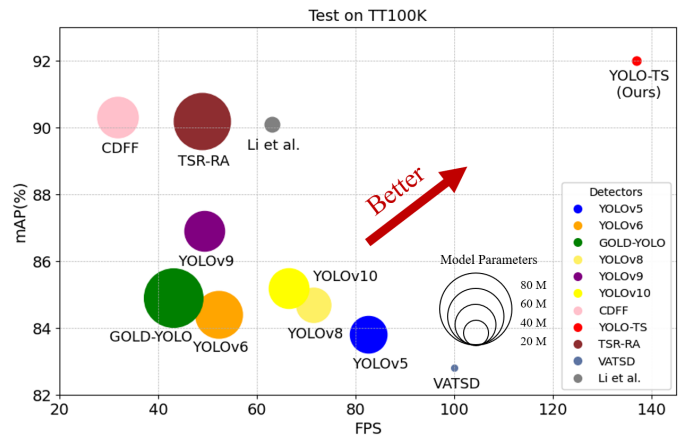


Fig. 2. Comparison of the speed and accuracy of different object detectors on TT100K.

validate the effectiveness of the proposed YOLO-TS detector. Our method achieves state-of-the-art performance, demonstrating superior accuracy and speed compared to existing approaches. Specifically, YOLO-TS not only surpasses previous methods in mean Average Precision (mAP) but also achieves the highest frames per second (FPS) rate while significantly reducing the model's parameter count.

II. RELATED WORK

This section reviews existing work pertinent to our research, with a focus on object detection methodologies, challenges in

small object detection, innovations in single-scale feature map prediction, and the use of dilated convolutions.

A. Object Detection

In recent years, continuous developments in the field of deep learning have significantly improved the performance of object detection algorithms, leading to the gradual obsolescence of traditional methods. Ross Girshick introduced R-CNN [23] in 2014, marking the first application of CNNs in object detection and pioneering the use of neural networks in this area. Modern object detection algorithms are typically categorized into two types: two-stage detectors, exemplified by the R-CNN series [1], [23], and one-stage detectors, exemplified by the YOLO series [24]–[30]. Two-stage detectors first extract candidate boxes from the image and then classify the contents within these boxes to achieve high-precision object detection. However, this method is relatively slow in detection speed. In contrast, one-stage detectors reformulate the object detection problem as a regression problem, directly predicting the target location and bounding box attributes from image pixels, significantly improving detection speed. This approach is particularly effective in fields such as vehicle, pedestrian, and traffic sign detection. Despite their efficacy, one-stage detectors' proficiency in small object detection remains sub-optimal.

B. Small Object Detection

Detecting small objects is a formidable challenge in object detection because their limited pixel representation makes them distinct from medium and large objects. This pixel limitation often results in a scarcity of feature information, leading to weak feature representations that hinder accurate detection and localization. The small size of these objects further complicates detection, as they can appear anywhere within an image, including in peripheral regions or amidst overlapping objects.

To enhance the detection accuracy of small objects, the research community has explored a variety of strategies. These include data augmentation [31]–[33], multi-scale fusion [34]–[37], leveraging contextual information [38]–[40], applying super-resolution techniques [41]–[44], and utilizing region proposals [45]–[47]. Each of these methods aims to empower convolutional neural networks with improved capability for feature extraction from small objects, thereby boosting detection performance.

A critical aspect of enhancing small object detection lies in optimizing the receptive field's size to align with the objects' dimensions and contextual backdrop. An overly small receptive field might fail to encapsulate adequate contextual details, leading to imprecise detection outcomes. Conversely, an excessively large receptive field could inadvertently encompass too much background noise, potentially leading to false positives or imprecise detections. Therefore, fine-tuning the dimensions of the receptive field becomes a crucial strategy for achieving accurate small object detection.

C. Single-Scale Feature Map Prediction

Traditional YOLO series algorithms [2], [26], [48], [49], typically based on an anchor-based method, generate multiple sets of preset anchor boxes to classify and adjust their positions, covering different sizes and shapes of targets on multi-scale feature maps. Another type of detector relies on the anchor-free method to directly regress the center points and dimensions of targets on different scale feature maps. FSAF [50] dynamically adjusts anchor points on the feature map, significantly enhancing the detection capability for various sizes of targets. YOLOF [51], an innovative anchor-free object detection algorithm, introduces a global information guidance module to more effectively utilize global contextual information on a single scale. CenterNet [52] adopts a more streamlined design, combining the target's center point with its width and height, achieving single-scale object detection. Compared to traditional multi-scale methods, the anchor-free method does not depend on predefined anchor boxes but directly predicts the location of targets in the image through the network. Simplifying our model design would be possible if we could directly predict multi-scale targets on a single-scale feature map rich in contextual information.

D. Dilated Convolution

Dilated convolution is widely used in computer vision tasks such as semantic segmentation and object detection [53]. Its main goal is to expand the receptive field and enhance the capture of contextual information from images while maintaining resolution. In practice, dilated convolution is utilized in two main forms: serial and parallel. Employing mixed dilated convolutions in series, such as Hybrid Dilated Convolution (HDC) [53], reduces the grid effect through varying dilation rates, while parallel methods like the Atrous Spatial Pyramid Pooling (ASPP) module in DeepLab [54] and the Receptive Field Block (RFB) module in RFBNet [55] combine convolutions with different dilation rates to fuse multi-scale features. However, these approaches exhibit limitations when addressing small-sized targets, as the grid effect caused by the use of dilated convolutions can lead to discontinuous regions within the feature map. The textural details of small objects may inadvertently fall within these discontinuous regions, adversely affecting the detection of small targets. For small object detection, finding a more effective balance between sensitivity to detail features and maintaining a large receptive field is necessary.

III. PROPOSED METHOD

A. Receptive Field Alignment in Multi-Scale Feature Maps

The efficacy of small object detection hinges on the nuanced alignment of receptive fields with the size distribution of objects. Prior research has extensively explored feature fusion techniques, yet it often underemphasizes the critical alignment between receptive field sizes and small objects in datasets. This alignment is pivotal, as objects of varied sizes demand distinct receptive field dimensions for optimal detection [56].

High-resolution feature maps, characterized by smaller receptive fields, are inherently adept at detecting smaller objects.

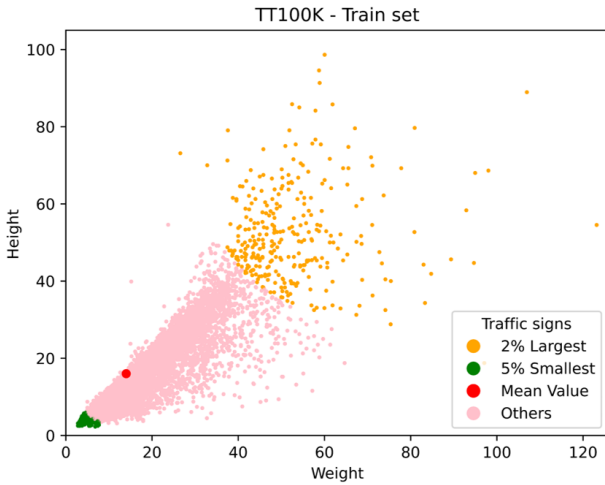


Fig. 3. The distribution of object anchor box sizes in the training set of TT100K.

Conversely, larger objects are more effectively detected using low-resolution feature maps, which possess larger receptive fields. As feature maps are downsampled, their receptive fields enlarge. However, a mismatch in receptive field size—whether too small or too large—can lead to incomplete feature capture or excessive irrelevant information. Hence, tuning the receptive field sizes at different scales is imperative for effective multi-scale object detection.

For this reason, we optimally set the receptive fields of feature maps at different scales to ensure they effectively match the size distribution of small objects, thereby optimizing the performance of small object detection. The formula for calculating the receptive field of convolutional layers is as follows [57]:

$$RF_n = RF_{n-1} + (K_n - 1) \times \prod_{i=1}^{n-1} S_i, \quad (1)$$

where K_n and S_n represent the kernel size and stride of the n^{th} layer, respectively. RF_{n-1} is the receptive field size of the previous layer.

Figure 3 illustrates the distribution of anchor box sizes within the TT100K training dataset, guiding the adjustment of receptive field sizes across different network scales. Specifically, the P1 layer is optimized for extracting features from very small signs, while subsequent layers (P2, P3, P4, and P5) are tailored for progressively larger signs. Considering that the practical receptive field tends to be smaller than its theoretical counterpart [58], we align the receptive fields of multiscale feature maps with the size distribution of smaller targets in the dataset using the following strategy:

$$P1_{RF} = \lambda \times \text{anchor}_{\text{tiny}} \quad (2)$$

$$P2_{RF} = \lambda \times (\text{anchor}_{\text{tiny}} + \text{anchor}_{\text{mean}}) \quad (3)$$

$$P3_{RF} = \lambda \times \text{anchor}_{\text{mean}} \quad (4)$$

$$P4_{RF} = \lambda \times (\text{anchor}_{\text{mean}} + \text{anchor}_{\text{large}}) \quad (5)$$

$$P5_{RF} = \lambda \times \ln(\text{anchor}_{\text{large}}) \quad (6)$$

TABLE I
DETAILS OF OUTPUT SIZES, C2F BLOCKS, AND RF SIZES FOR YOLO-TS LAYERS

Feature map	Output size	C2F blocks	RF size
Input	640×640	-	1
P1	320×320	3	27
P2	160×160	1	47
P3	80×80	1	87
P4	40×40	1	167
P5	20×20	1	327

where $P1_{RF}$, $P2_{RF}$, $P3_{RF}$, $P4_{RF}$, and $P5_{RF}$ represent the theoretical receptive fields of each respective layer. λ is a tunable hyperparameter, and $\text{anchor}_{\text{tiny}}$, $\text{anchor}_{\text{large}}$, and $\text{anchor}_{\text{mean}}$ correspond to the average dimensions of the smallest 5%, largest 2%, and the overall mean of object sizes in the dataset.

To validate the choice of λ , we conducted extensive experiments comparing different values of λ . The results showed that our chosen λ significantly improved the mAP50 for small object detection compared to other values. These findings demonstrate that our receptive field alignment strategy, optimized through the selection of λ , effectively balances feature map resolution and receptive field size, optimizing the performance of small object detection.

By adjusting the number of Block modules within the C2F module for different scale feature maps in the backbone, we can fine-tune the network depth, thereby altering the size of the receptive fields for feature maps at various scales. Table I provides detailed information on the output sizes for layers P1 to P5, the number of Blocks in the C2F module, the theoretical receptive field sizes, and the detection size ranges. This meticulous adjustment ensures accurate detection across scales, significantly enhancing small object detection precision.

B. High-Resolution Feature Map for Multi-Scale Detection

In the realm of convolutional neural networks (CNNs), large-scale feature maps are fundamentally equipped to detect small objects, thanks to their smaller receptive fields which are critical for preserving the granular details of diminutive targets. This attribute makes them inherently preferable for identifying small-scale objects, such as traffic signs, when compared to feature maps derived through successive downsampling, which tend to lose information pertinent to such small entities. However, a drawback of relying solely on large-scale feature maps is their restricted capacity to encapsulate extensive semantic feature information, rendering the direct prediction of multi-scale targets potentially less effective due to the suboptimal extraction of pertinent features.

Conventionally, a Feature Pyramid Network (FPN) [59] is leveraged to enrich the semantic depth of the P2 layer through top-down multi-layer information fusion. However, a limitation of the FPN structure is that it can only fully integrate the features of adjacent layers, and for inter-layer information, it can only be indirectly obtained through a recursive method [27]. This causes the information of a certain layer to primarily support its adjacent layers, with limited contributions to other

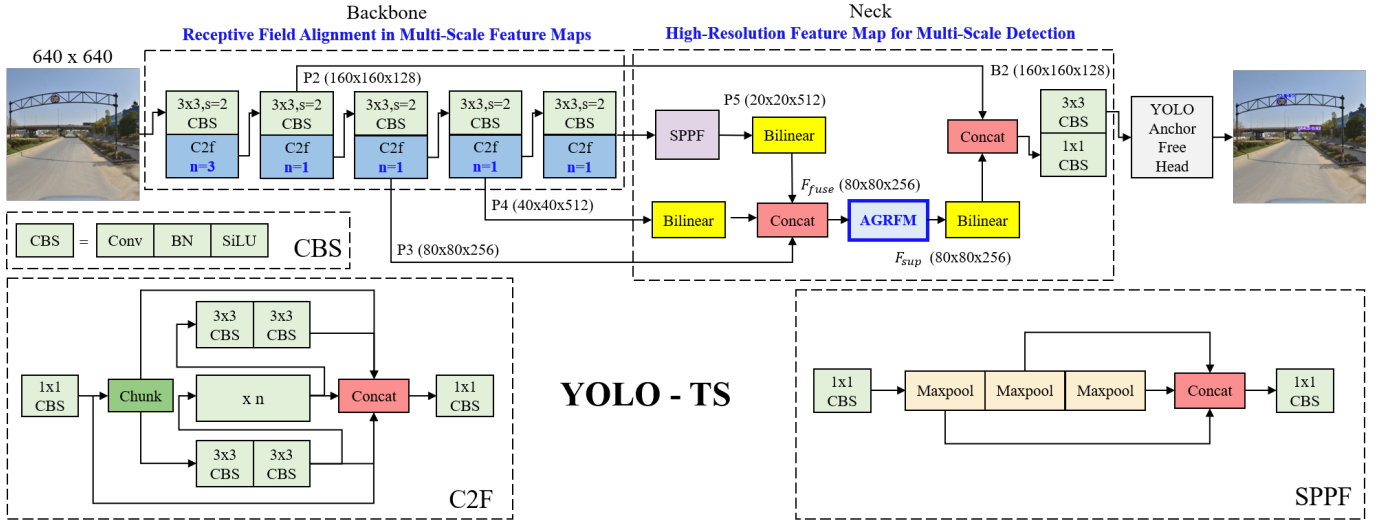


Fig. 4. The structure of YOLO-TS.

layers, potentially restricting the overall effect of information fusion.

To mitigate the loss of cross-layer information transmission within the FPN, we introduce and enhance an advanced feature fusion mechanism, as depicted in Fig. 4. We utilized bilinear interpolation operation to upsample the input features from layers P4 and P5, aligning their size with that of layer P3. By directly merging features from different levels to obtain supplementary layer information, and then infusing this supplementary information into the large-scale feature layer P2 to obtain the final high-resolution feature map B2, which contains rich contextual information. This approach has significantly enhanced the model's detection accuracy for targets of large, medium, and small sizes. The feature fusion mechanism can be summarized as follows:

$$F_{fuse} = \text{Concat}(\text{Bilinear}(P5), \text{Bilinear}(P4), P3) \quad (7)$$

$$F_{sup} = \text{AGRFM}(F_{fuse}) \quad (8)$$

$$F_{B2} = \text{Concat}(\text{Bilinear}(F_{sup}, P2)) \quad (9)$$

C. Anti-Grid Receptive Field Module

Dilated convolution, an extension of traditional convolution, allows networks to expand their receptive fields without increasing computational complexity. However, the use of dilated convolutions with high dilation rates, either singly or in sequence, can lead to a gridding effect. This effect may create regions of discontinuity in feature maps. Some texture details of small objects may fall right into these discontinuous regions, which is detrimental to the detection of small objects.

In contrast, standard convolution layers (non-dilated) can cover continuous pixel areas and capture information between adjacent pixels despite their limited receptive fields. This results in continuous and smooth feature representations on the feature maps. Such smooth representations effectively complement dilated convolutions, providing a seamless transition on the feature map. Therefore, we explore combining the

advantages of standard and dilated convolutions to eliminate the gridding effect associated with dilated convolutions.

Employing multiple consecutive standard convolutions effectively acts like a larger convolution kernel through the overlay of smaller kernels. This increases the usage frequency of pixels in the central area compared to those on the edges. Subsequently, applying high dilation rate convolutions spreads the pixel usage frequency. If the dilation rate is too high, the dilated convolution kernels might create multiple, distinctly spaced high-frequency usage areas on the feature map. To prevent the final dilated convolution from creating several small, spaced-out areas, we need to select a moderate dilation rate. This ensures that the final dilated convolution covers no more than all the pixels previously covered by the effective large kernel of the prior standard convolutions. Otherwise, the final dilated convolution will use pixels not covered by the preceding effective large kernel, leading to the phenomenon of multiple closely spaced areas. The following condition should be met:

$$(k-1) \times r + 1 < k', \quad (10)$$

where k and r are the size and the dilation rate of the last dilated convolution kernel. k' is the equivalent kernel size of all previous standard convolutions.

Figure 5 illustrates the pixel utilization frequency statistics in feature maps obtained through different combinations of dilated convolution layers. We observe that continuous use of high dilation rates easily produces a significant grid effect. The combination of multiple standard convolutional layers with a single appropriate atrous convolutional layer not only reduces the usage frequency of central pixels but also encourages the frequent utilization of more widely distributed pixels. This effectively avoids the grid effect while enhancing the receptive field while maintaining the continuity of feature maps. If the condition proposed in equation 10 is not met, it will result in the phenomenon of multiple closely spaced areas as shown in Fig. 5(e).

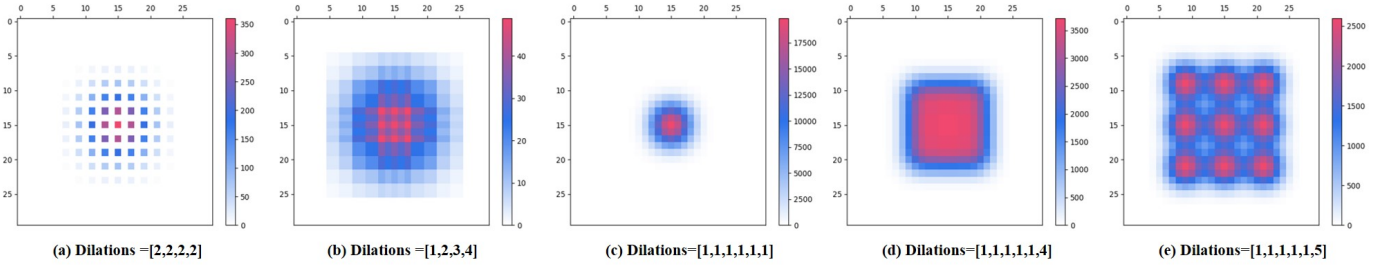


Fig. 5. Pixel utilization frequency statistics in feature maps: (a) Pixel utilization frequency statistics in feature map obtained by cascading four 3×3 convolutions with a dilation rate of 2. (b) Pixel utilization frequency statistics in feature map obtained by cascading four 3×3 convolutions with dilation rates of 1, 2, 3, and 4. (c) Pixel utilization frequency statistics in feature map obtained by cascading six 3×3 convolutions with a dilation rate of 1. (d) Pixel utilization frequency statistics in feature map obtained by cascading five 3×3 convolutions with a dilation rate of 1 and one 3×3 convolution with a dilation rate of 4. (e) Pixel utilization frequency statistics in feature map obtained by cascading five 3×3 convolutions with a dilation rate of 1 and one 3×3 convolution with a dilation rate of 5.

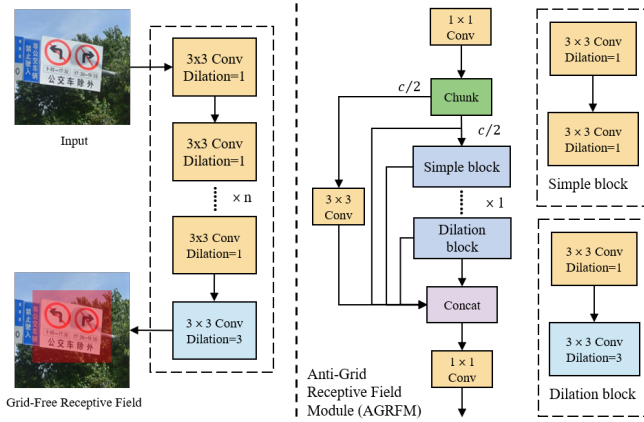


Fig. 6. The structure of Anti-Grid Receptive Field Module(AGRFM)

Inspired by the multi-gradient flow connections in the C2F module, we designed the AGRFM, as shown in Fig. 6. We split the input into two paths: one undergoing standard convolution operations and the other passing through a sequence of standard convolution layers followed by a high-dilation-rate convolution layer. This approach mitigates the grid effect introduced by dilated convolutions and achieves information extraction from coarse to fine during the detection process. This strategy not only ensures model efficiency but also enhances the effectiveness of information utilization by capturing a broader context. Consequently, it significantly improves the model's detection capability for targets of various sizes and detail levels.

IV. EXPERIMENTS

In this section, we conduct a comprehensive validation of our proposed method. We also evaluate the effectiveness of our receptive field alignment in multi-scale feature maps, high-resolution feature map for multi-scale detection, and the AGRFM. We then compare our detector's performance with other state-of-the-art detectors.

A. Experimental settings

1) *Datasets*: Our model has been performance-validated across several public benchmark datasets, including TT100K

[21] and CCTSDB2021 [22]. The TT100K dataset, sourced from Tencent Street View Maps, includes 100,000 images with a resolution of 2048×2048 pixels. Of these, 10,000 annotated images feature 30,000 traffic signs. The CCTSDB2021 dataset, developed by Changsha University of Science and Technology in China, comprises 17,856 images in the training and test sets, with traffic signs classified as mandatory, prohibitory, or warning types. There are 16,356 training images, numbered from 00000 to 18991, and 1,500 test images, numbered from 18992 to 20491.

The TT100K dataset comprises around 150 traffic sign categories. Using the approach of Zhu et al. [21], we excluded categories with fewer than 100 samples, narrowing the focus to 45 categories. The number of instances for each category is shown in Fig. 7. This benchmark dataset is accessible at <http://cg.cs.tsinghua.edu.cn/traffic-sign/>. The training set includes 6,105 images, each with a resolution of 2048×2048 pixels, and approximately 15,000 traffic signs across the 45 categories. The test set consists of 3,071 images with the same resolution, containing 7,070 traffic signs.

2) *Evaluation metrics*: Similar to previous traffic sign detection methods, we evaluate the performance of the proposed algorithm using Precision, Recall, F1 score, mean Average Precision at 50% IoU (mAP50), and speed (FPS). These metrics are calculated using the following formulas:

$$Precision = \frac{TP}{TP + FP} \quad (11)$$

$$Recall = \frac{TP}{TP + FN} \quad (12)$$

$$F1 = \frac{2 \times Precision \times Recall}{Precision + Recall} \quad (13)$$

$$mAP50 = \frac{1}{N} \sum_{i=1}^N AP_{50}^i \quad (14)$$

where TP is the count of true positive traffic sign detections, FP is the count of false positives, FN is the count of false negatives where traffic signs are present but undetected, N represents the total number of categories, and AP_{50}^i indicates the average precision at 50% IoU for each category.

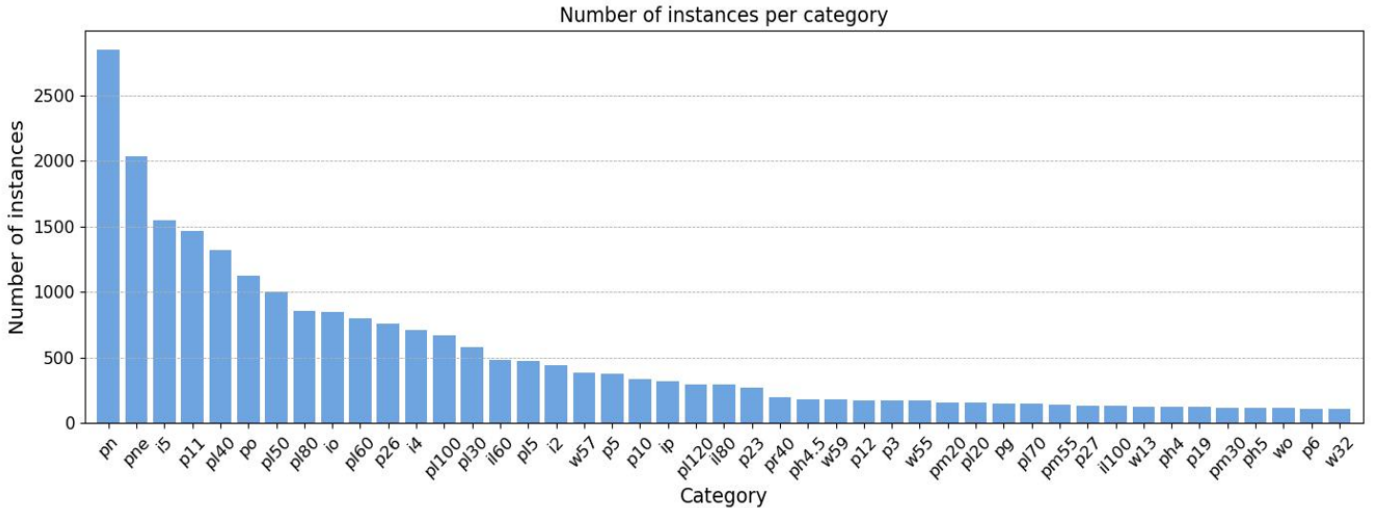


Fig. 7. Number of instances per category in TT100K for classes with more than 100 instances

TABLE II

PERFORMANCE COMPARISON ON TT100K DATASET; THE FIRST AND SECOND BEST RESULTS ARE INDICATED IN BLUE AND GREEN, RESPECTIVELY.

Method	Venue	Input Size	Precision(%)	Recall(%)	F1	Params(M)	GFLOPs	mAP50(%)	FPS	GPU
TSR-SA [4]	NCA2021	608×608	-	-	-	-	-	90.2	48.8	V100
CDFD [60]	NCA2022	608×608	-	-	-	-	-	90.3	31.8	TITAN V
I2D-Net [61]	TIM2023	512×512	-	-	-	87.5	-	71.6	-	RTX 2070
Zhang et al. [62]	TETCI2024	640×640	-	-	-	81.3	95.0	70.2	-	RTX 2080Ti
VATSD [63]	TITS2024	608×608	-	-	-	7.9	16.6	82.8	100.0	RTX 3080
Li et al. [64]	TITS2024	640×640	-	-	-	-	-	90.1	63.0	TITAN XP
YOLOv5-L [24]	2020	640×640	82.0	78.3	0.801	46.5	109.1	83.8	82.6	RTX 3090
YOLOv6-L [25]	CVPR2022	640×640	84.5	76.0	0.800	59.6	150.7	84.4	52.2	RTX 3090
GOLD-YOLO-L [27]	NeurIPS2023	640×640	83.1	77.5	0.802	75.1	151.7	84.9	43.0	RTX 3090
YOLOv8-L [28]	2023	640×640	83.4	77.2	0.802	43.6	165.4	84.7	71.4	RTX 4090
YOLOv9-C [29]	CVPR2024	640×640	85.1	79.0	0.819	51.1	239.4	86.5	49.3	RTX 4090
YOLOv10-L [30]	2024	640×640	84.4	77.7	0.809	25.9	127.6	85.2	66.5	RTX 4090
ours	-	640×640	89.1↑	86.1↑	0.876↑	11.1	99.1	92.0↑	137.0↑	RTX 4090

3) *Training details*: The experimental setup includes a machine equipped with NVIDIA GeForce RTX 4090 GPUs. We use YOLOv8 as our baseline, with methods implemented in PyTorch. The optimizer’s learning schedule and settings align with those of YOLOv8, using Stochastic Gradient Descent (SGD) with a 0.01 learning rate and 0.937 momentum. The model is trained for 200 epochs with a batch size of 48, starting from scratch without any pre-trained weights.

B. Comparisons with the state-of-the-arts

Table II presents the experimental outcomes on the TT100K dataset, demonstrating that our approach attains state-of-the-art performance on multiple critical metrics. Specifically, our model achieved a precision of 89.1% and a recall of 86.1%, demonstrating superior recognition accuracy and the ability to reliably detect a greater number of correct traffic sign categories. On the critical mAP50 metric, our approach outperforms the previous best model [60], which had an mAP50 of 90.3%, achieving a new high of 92.0%. This highlights

that our algorithm significantly enhances detection accuracy, providing a safeguard for autonomous driving safety. Most notably, compared to the previous state-of-the-art methods, our approach not only significantly improves the mAP50 but also greatly enhances the FPS, achieving an impressive FPS metric of 137.0. Figure 8 presents a comparison of the effectiveness of our method against YOLOv8 and YOLOv9 in detecting traffic signs, which gives us an intuitive impression of the high performance of the proposed method.

Table III shows the experimental results on the CCTSDB2021 dataset. Our model outperforms other advanced YOLO series detectors, including the powerful YOLOv9-C, achieving an mAP50 of 88.7%. This represents an improvement over the previous best model [62], which had an mAP50 of 87.6%. Furthermore, with only 12.9M parameters, our model significantly reduces model complexity while greatly optimizing computational efficiency and resource usage. These results demonstrate the superior performance of our method and its considerable potential for practical applications.

TABLE III
PERFORMANCE COMPARISON ON CCTSDB2021 DATASET; THE FIRST AND SECOND BEST RESULTS ARE INDICATED IN BLUE AND GREEN, RESPECTIVELY.

Method	Venue	Input Size	Precision(%)	Recall(%)	F1	Param(M)	GFLOPs	mAP50(%)	FPS	GPU
Zhang et al. [62]	TETCI 2024	640×640	-	-	-	81.3	95.0	87.6	-	RTX 2080Ti
YOLOv5-L [24]	2020	640×640	91.3	75.7	0.828	46.5	109.1	82.1	107.5	RTX 4090
YOLOv6-L [25]	CVPR2022	640×640	90.0	78.6	0.839	59.6	150.7	84.4	75.4	RTX 4090
GOLD-YOLO-L [27]	NeurIPS2023	640×640	88.6	79.3	0.837	75.1	151.7	84.2	43.4	RTX 3090
YOLOv8-L [28]	2023	640×640	89.0	76.6	0.823	43.6	165.4	84.3	90.9	RTX 4090
YOLOv9-C [29]	CVPR2024	640×640	88.0	78.9	0.832	51.1	239.4	84.6	48.3	RTX 4090
YOLOv10-L [30]	2024	640×640	88.5	75.9	0.817	25.8	127.2	82.2	76.4	RTX 4090
ours	-	640×640	90.1	81.5 ↑	0.856 ↑	12.9	120.2	88.7 ↑	147.1 ↑	RTX 4090

TABLE IV
ABLATION STUDY FOR DIFFERENT COMPONENTS OF YOLO-TS ON TT100K. THE BEST RESULT IS MARKED IN BLUE.

Model	RFA-M	HR-MSD	AGRFM	Params(M)	GFLOPs	mAP50(%)	FPS
Baseline				43.6	165.0	84.7	71.4
	✓			32.8	127.7	88.0	89.3
		✓		20.8	121.8	90.6	111.1
	✓	✓		9.8	83.8	91.5	156.3
		✓	✓	21.9	137.2	90.2	101.0
Ours	✓	✓	✓	11.1	99.1	92.0 ↑	137.0

TABLE V
ABLATION STUDY ON DIFFERENT VALUES OF λ FOR RECEPTIVE FIELD ALIGNMENT IN MULTI-SCALE FEATURE MAPS. THE BEST RESULT IS MARKED IN BLUE.

λ	Params(M)	GFLOPs	mAP50(%)
1	11.0	90.6	91.6
2	11.0	90.6	91.6
3	11.0	94.9	91.7
4	11.1	99.1	92.0 ↑
5	11.2	103.3	91.9
6	12.5	111.8	91.8

C. Ablation Study

This section presents ablation experiments to verify the effectiveness of each component in our proposed method, using the challenging TT100K dataset for quantitative analysis.

1) *Effectiveness of Receptive Field Alignment in Multi-Scale Feature Maps (RFA-M)*: To assess the effectiveness of RFA-M, we conducted the corresponding ablation study as shown in the second row of Table IV. RFA-M maintains a high mAP50 while effectively simplifying the network architecture. Specifically, RFA-M reduces the model’s parameters from 43.6M to 32.8M and GFLOPs from 165.0 to 127.7, while increasing the mAP50 to 88.0% and the FPS to 89.3. This demonstrates that RFA-M not only simplifies the network architecture but also enhances detection performance.

2) *Different values of λ in the Receptive Field Alignment in Multi-Scale Feature Maps (RFA-M)*: To validate the selection of the hyperparameter λ , we conducted an ablation study. As shown in Table V, the mAP50 improves as λ increases from 1 to 4, peaking at 92.0% when $\lambda=4$. Beyond this value, the mAP50 decreases despite the number of parameters and GFLOPs increase. This indicates that $\lambda=4$ achieves the optimal

TABLE VI
ABLATION STUDY ON DIFFERENT DILATIONS OF THE LAST CONVOLUTION IN THE DILATION BLOCK. THE BEST RESULT IS MARKED IN BLUE.

Dilation rates	Precision(%)	Recall(%)	F1	mAP50(%)
d=1	89.4	84.9	0.871	91.6
d=2	88.5	85.9	0.872	91.8
d=3	89.1	86.1	0.876	92.0 ↑
d=4	88.7	85.5	0.871	91.7
d=5	87.0	86.7	0.868	91.1

balance between model complexity and detection performance. This optimal value ensures that the receptive fields are well-aligned with the size distribution of objects in the dataset, particularly enhancing the detection performance for small objects by capturing sufficient contextual details without introducing excessive background noise.

3) *Effectiveness of High-Resolution Feature Map for Multi-Scale Detection (HR-MSD)*: To assess the effectiveness of HR-MSD, we conducted corresponding ablation experiments, as indicated in Table IV. Upon incorporating HR-MSD, both mAP50 and FPS experienced significant improvements, and the FPS impressively reached 111.1. This demonstrates that HR-MSD substantially enhances the model’s recognition capability and significantly increases the speed of detection. These results indicate that the use of high-resolution feature maps not only preserves detailed information necessary for accurate detection of small objects but also improves the overall efficiency and responsiveness of the detection model.

4) *Effectiveness of AGRFM*: To evaluate the effectiveness of AGRFM, we conducted the corresponding ablation experiment as shown in the fourth row of Table IV. The incorporation of AGRFM significantly expanded the receptive field after multi-scale feature map fusion. As shown in the last two rows of Table IV, when AGRFM is used in conjunction with the HR-MSD, the mAP50 is improved to 92.0%, ensuring that the model achieves high-precision detection across a wide range of traffic sign categories. Moreover, this combination also achieves a high FPS of 137.0, demonstrating that the use of AGRFM can maintain a high speed while effectively enhancing accuracy when combined with RFA-M and HR-MSD.



Fig. 8. Traffic sign detection results on the TT100K dataset.

5) *Different dilation rates of the Dilation Block in AGRFM*: To determine the optimal receptive field expansion, we replaced the last dilated convolution in the Dilation Block of AGRFM with dilated convolutions of different dilation rates. The results of varying the dilation rates of the last convolution in the dilation block are presented in Table VI. Using dilated convolutions with higher dilation rates, the performance of YOLO-TS improved. However, when the dilation rate is too high, the improvement saturates and may even lead to a decrease in accuracy. This is likely due to the fact that a

dilation rate of three is sufficient to match the scale of all objects in the images. Furthermore, if the last dilation rate does not meet the criteria of Equation 10, as shown in Table VI, when $d=5$, the detection accuracy actually decreases. This underscores that an excessively high dilation rate can adversely affect the detection accuracy of small objects by causing the grid effect, which negatively impacts the precision of detecting small objects.

TABLE VII
PERFORMANCE COMPARISON ON CCTSDB2021 DATASET ON THE MOBILE EDGE DEVICE. * MEANS THE RESULT AFTER ACCELERATED INFERENCE WITH TENSORRT 8 AND FP16. THE FIRST AND SECOND BEST RESULTS ARE INDICATED IN BLUE AND GREEN, RESPECTIVELY.

Method	Venue	Input Size	mAP50(%)	FPS	mAP50(%)*	FPS*	Device
YOLOv5-L [24]	2020	640×640	82.1	41.1	82.0	57.6	NVIDIA Jetson AGX Orin
YOLOv6-L [25]	CVPR2022	640×640	84.0	24.2	83.3	30.7	
GOLD-YOLO-L [27]	NeurIPS2023	640×640	83.8	20.0	83.0	28.5	
YOLOv8-L [28]	2023	640×640	84.3	37.6	84.3	48.3	
YOLOv9-C [29]	CVPR2024	640×640	85.2	17.9	85.2	44.4	
YOLOv10-L [30]	2024	640×640	82.2	27.2	82.0	80.6	
ours	-	640×640	88.7 ↑	38.8	88.6 ↑	53.2	

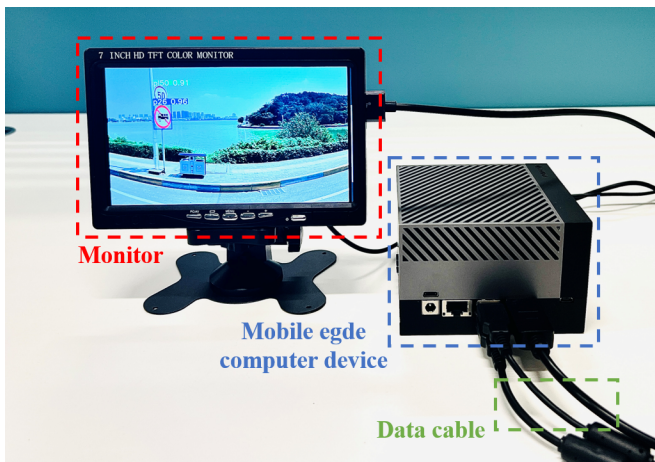


Fig. 9. Mobile Edge Computing Device NVIDIA Jetson AGX Orin.

V. COMPARISON OF INFERENCE SPEED

In this section, we conducted a comprehensive assessment of the inference speeds of our YOLO-TS model relative to other advanced methods. The tests were conducted on NVIDIA’s high-end GPUs and on the mobile edge device NVIDIA Jetson AGX Orin, as shown in Fig. 9. The latter utilizes the TensorRT 8 FP16 inference acceleration framework. TensorRT can convert PyTorch deep learning models into optimized TensorRT engines, enhancing the inference performance and efficiency of models deployed on NVIDIA edge devices through techniques such as layer fusion, precision calibration, and memory optimization.

Our evaluations utilized a validation set composed of 1,500 images from the CCTSDB-2021 dataset, with batch size consistently set at 1. The results, presented in Table III and Table VII, demonstrate that YOLO-TS not only achieves the highest accuracy but also delivers formidable real-time inference speeds on various platforms. Specifically, on NVIDIA GPUs, YOLO-TS achieves an inference speed of up to 147.1 FPS, outperforming models such as YOLOv9-C and YOLOv10-L. On the NVIDIA Jetson AGX Orin, with the support of TensorRT 8 FP16 optimization, YOLO-TS achieved 53.2 FPS. This substantial boost in processing speed, particularly on edge devices, is vital for real-time applications in Autonomous Driving Systems (ADS) and Advanced Driver-Assistance Sys-

tems (ADAS), where fast and precise data processing is imperative.

VI. CONCLUSION AND FUTURE WORK

In this study, we introduced YOLO-TS, an efficient and real-time traffic sign detection network inspired by the YOLO (You Only Look Once) series models, specifically designed for detecting small traffic signs. Our design emphasizes the crucial role of the receptive field in detecting small objects, optimizing the model architecture by aligning the receptive field with the size of small targets to enhance detection speed and accuracy. By fusing multi-scale feature map receptive fields into a single high-resolution feature map rich in contextual information, we leverage the flexibility of the anchor-free approach to support precise detection of multi-scale targets. Additionally, we mitigated the potential grid effect caused by atrous convolutions through the Anti-Grid Receptive Field Module (AGRFM), which combines multiple standard convolution layers with a single dilation convolution layer. This approach enhances pixel utilization and maintains feature map continuity, significantly improving detection accuracy. Our experiments on the TT100K and CCTSDB2021 datasets show that YOLO-TS achieves state-of-the-art performance, significantly enhancing traffic sign detection for real-time applications like autonomous driving and advanced driver-assistance systems.

In future work, expanding the dataset to include more diverse and challenging scenarios will be crucial, such as adverse weather conditions, road signs from different countries, and dynamically changing environments. This expansion will enhance the model’s robustness and generalization, ensuring its effectiveness across different regions and in suboptimal conditions. By increasing the diversity of the dataset, we can further optimize and adjust the network to cope with the complex and variable real-world application scenarios, thereby providing more accurate and reliable road sign detection in autonomous driving and advanced driver-assistance systems.

We would like to release our source code.

REFERENCES

- [1] S. Ren, K. He, R. Girshick, and J. Sun, “Faster r-cnn: Towards real-time object detection with region proposal networks,” *IEEE transactions on pattern analysis and machine intelligence*, vol. 39, no. 6, pp. 1137–1149, 2016.

- [2] J. Redmon, S. Divvala, R. Girshick, and A. Farhadi, "You only look once: Unified, real-time object detection," in *Proceedings of the IEEE conference on computer vision and pattern recognition*, 2016, pp. 779–788.
- [3] J. Yu, X. Ye, and Q. Tu, "Traffic sign detection and recognition in multimaps using a fusion model with yolo and vgg network," *IEEE Transactions on Intelligent Transportation Systems*, vol. 23, no. 9, pp. 16 632–16 642, 2022.
- [4] J. Chen, K. Jia, W. Chen, Z. Lv, and R. Zhang, "A real-time and high-precision method for small traffic-signs recognition," *Neural Computing and Applications*, vol. 34, no. 3, pp. 2233–2245, 2022.
- [5] W. Min, R. Liu, D. He, Q. Han, Q. Wei, and Q. Wang, "Traffic sign recognition based on semantic scene understanding and structural traffic sign location," *IEEE Transactions on Intelligent Transportation Systems*, vol. 23, no. 9, pp. 15 794–15 807, 2022.
- [6] J. Wang, Y. Chen, Z. Dong, and M. Gao, "Improved yolov5 network for real-time multi-scale traffic sign detection," *Neural Computing and Applications*, vol. 35, no. 10, pp. 7853–7865, 2023.
- [7] M. Hassaballah, M. A. Kenk, K. Muhammad, and S. Minaee, "Vehicle detection and tracking in adverse weather using a deep learning framework," *IEEE transactions on intelligent transportation systems*, vol. 22, no. 7, pp. 4230–4242, 2020.
- [8] G. Li, Z. Ji, and X. Qu, "Stepwise domain adaptation (sda) for object detection in autonomous vehicles using an adaptive centernet," *IEEE Transactions on Intelligent Transportation Systems*, vol. 23, no. 10, pp. 17 729–17 743, 2022.
- [9] R. S. Charran and R. K. Dubey, "Two-wheeler vehicle traffic violations detection and automated ticketing for indian road scenario," *IEEE Transactions on Intelligent Transportation Systems*, vol. 23, no. 11, pp. 22 002–22 007, 2022.
- [10] L. Chen, S. Lin, X. Lu, D. Cao, H. Wu, C. Guo, C. Liu, and F.-Y. Wang, "Deep neural network based vehicle and pedestrian detection for autonomous driving: A survey," *IEEE Transactions on Intelligent Transportation Systems*, vol. 22, no. 6, pp. 3234–3246, 2021.
- [11] W.-Y. Hsu and P.-Y. Yang, "Pedestrian detection using multi-scale structure-enhanced super-resolution," *IEEE Transactions on Intelligent Transportation Systems*, 2023.
- [12] H. Xu, M. Guo, N. Nedjah, J. Zhang, and P. Li, "Vehicle and pedestrian detection algorithm based on lightweight yolov3-promote and semi-precision acceleration," *IEEE Transactions on Intelligent Transportation Systems*, vol. 23, no. 10, pp. 19 760–19 771, 2022.
- [13] X. Zhou and L. Zhang, "Sa-fpn: An effective feature pyramid network for crowded human detection," *Applied Intelligence*, vol. 52, no. 11, pp. 12 556–12 568, 2022.
- [14] Y. Cai, T. Luan, H. Gao, H. Wang, L. Chen, Y. Li, M. A. Sotelo, and Z. Li, "Yolov4-5d: An effective and efficient object detector for autonomous driving," *IEEE Transactions on Instrumentation and Measurement*, vol. 70, pp. 1–13, 2021.
- [15] X. Zhu, S. Lyu, X. Wang, and Q. Zhao, "Tph-yolov5: Improved yolov5 based on transformer prediction head for object detection on drone-captured scenarios," in *Proceedings of the IEEE/CVF international conference on computer vision*, 2021, pp. 2778–2788.
- [16] S. Li, Y. Li, Y. Li, M. Li, and X. Xu, "Yolo-firi: Improved yolov5 for infrared image object detection," *IEEE access*, vol. 9, pp. 141 861–141 875, 2021.
- [17] W. Sun, L. Dai, X. Zhang, P. Chang, and X. He, "Rsod: Real-time small object detection algorithm in uav-based traffic monitoring," *Applied Intelligence*, pp. 1–16, 2022.
- [18] Y. Li, Q. Fan, H. Huang, Z. Han, and Q. Gu, "A modified yolov8 detection network for uav aerial image recognition," *Drones*, vol. 7, no. 5, p. 304, 2023.
- [19] N. Zeng, P. Wu, Z. Wang, H. Li, W. Liu, and X. Liu, "A small-sized object detection oriented multi-scale feature fusion approach with application to defect detection," *IEEE Transactions on Instrumentation and Measurement*, vol. 71, pp. 1–14, 2022.
- [20] CleanPNG, <https://www.cleanpng.com/>, accessed: 2024.
- [21] Z. Zhu, D. Liang, S. Zhang, X. Huang, B. Li, and S. Hu, "Traffic-sign detection and classification in the wild," in *Proceedings of the IEEE conference on computer vision and pattern recognition*, 2016, pp. 2110–2118.
- [22] J. Zhang, X. Zou, L.-D. Kuang, J. Wang, R. S. Sherratt, and X. Yu, "Ctsdb 2021: a more comprehensive traffic sign detection benchmark," *Human-centric Computing and Information Sciences*, vol. 12, 2022.
- [23] R. Girshick, J. Donahue, T. Darrell, and J. Malik, "Rich feature hierarchies for accurate object detection and semantic segmentation," in *Proceedings of the IEEE conference on computer vision and pattern recognition*, 2014, pp. 580–587.
- [24] G. Jocher, "YOLOv5 by Ultralytics," May 2020. [Online]. Available: <https://github.com/ultralytics/yolov5>
- [25] C. Li, L. Li, H. Jiang, K. Weng, Y. Geng, L. Li, Z. Ke, Q. Li, M. Cheng, W. Nie *et al.*, "Yolov6: A single-stage object detection framework for industrial applications," *arXiv preprint arXiv:2209.02976*, 2022.
- [26] C.-Y. Wang, A. Bochkovskiy, and H.-Y. M. Liao, "Yolov7: Trainable bag-of-freebies sets new state-of-the-art for real-time object detectors," in *Proceedings of the IEEE/CVF conference on computer vision and pattern recognition*, 2023, pp. 7464–7475.
- [27] C. Wang, W. He, Y. Nie, J. Guo, C. Liu, Y. Wang, and K. Han, "Gold-yolo: Efficient object detector via gather-and-distribute mechanism," *Advances in Neural Information Processing Systems*, vol. 36, 2024.
- [28] G. Jocher, A. Chaurasia, and J. Qiu, "Ultralytics YOLO," Jan. 2023. [Online]. Available: <https://github.com/ultralytics/ultralytics>
- [29] C.-Y. Wang, I.-H. Yeh, and H.-Y. M. Liao, "Yolov9: Learning what you want to learn using programmable gradient information," *arXiv preprint arXiv:2402.13616*, 2024.
- [30] A. Wang, H. Chen, L. Liu, K. Chen, Z. Lin, J. Han, and G. Ding, "Yolov10: Real-time end-to-end object detection," *arXiv preprint arXiv:2405.14458*, 2024.
- [31] J. Zhang, Z. Xie, J. Sun, X. Zou, and J. Wang, "A cascaded r-cnn with multiscale attention and imbalanced samples for traffic sign detection," *IEEE access*, vol. 8, pp. 29 742–29 754, 2020.
- [32] J. Tang, J. Cheng, D. Xiang, and C. Hu, "Large-difference-scale target detection using a revised bhattacharyya distance in sar images," *IEEE Geoscience and Remote Sensing Letters*, vol. 19, pp. 1–5, 2022.
- [33] H. Zhou, A. Ma, Y. Niu, and Z. Ma, "Small-object detection for uav-based images using a distance metric method," *Drones*, vol. 6, no. 10, p. 308, 2022.
- [34] G. Qi, Y. Zhang, K. Wang, N. Mazur, Y. Liu, and D. Malaviya, "Small object detection method based on adaptive spatial parallel convolution and fast multi-scale fusion," *Remote Sensing*, vol. 14, no. 2, p. 420, 2022.
- [35] K. Hu, M. Li, M. Xia, and H. Lin, "Multi-scale feature aggregation network for water area segmentation," *Remote Sensing*, vol. 14, no. 1, p. 206, 2022.
- [36] D. He, Y. Qiu, J. Miao, Z. Zou, K. Li, C. Ren, and G. Shen, "Improved mask r-cnn for obstacle detection of rail transit," *Measurement*, vol. 190, p. 110728, 2022.
- [37] S. Li, K. Li, Y. Qiao, and L. Zhang, "A multi-scale cucumber disease detection method in natural scenes based on yolov5," *Computers and Electronics in Agriculture*, vol. 202, p. 107363, 2022.
- [38] X. Tang, D. K. Du, Z. He, and J. Liu, "Pyramidbox: A context-assisted single shot face detector," in *Proceedings of the European conference on computer vision (ECCV)*, 2018, pp. 797–813.
- [39] B. Li, C. Xiao, L. Wang, Y. Wang, Z. Lin, M. Li, W. An, and Y. Guo, "Dense nested attention network for infrared small target detection," *IEEE Transactions on Image Processing*, vol. 32, pp. 1745–1758, 2022.
- [40] T. Zhang, L. Li, S. Cao, T. Pu, and Z. Peng, "Attention-guided pyramid context networks for detecting infrared small target under complex background," *IEEE Transactions on Aerospace and Electronic Systems*, 2023.
- [41] J. Rabbi, N. Ray, M. Schubert, S. Chowdhury, and D. Chao, "Small-object detection in remote sensing images with end-to-end edge-enhanced gan and object detector network," *Remote Sensing*, vol. 12, no. 9, p. 1432, 2020.
- [42] Y. Wang, S. M. A. Bashir, M. Khan, Q. Ullah, R. Wang, Y. Song, Z. Guo, and Y. Niu, "Remote sensing image super-resolution and object detection: Benchmark and state of the art," *Expert Systems with Applications*, vol. 197, p. 116793, 2022.
- [43] J. Zhang, J. Lei, W. Xie, Z. Fang, Y. Li, and Q. Du, "Superyolo: Super resolution assisted object detection in multimodal remote sensing imagery," *IEEE Transactions on Geoscience and Remote Sensing*, vol. 61, pp. 1–15, 2023.
- [44] Y. Teng, J. Zhang, and L. Liu, "Msr-rcnn: a multi-class crop pest detection network based on a multi-scale super-resolution feature enhancement module," *Frontiers in Plant Science*, vol. 13, p. 810546, 2022.
- [45] Y. Yu, K. Zhang, L. Yang, and D. Zhang, "Fruit detection for strawberry harvesting robot in non-structural environment based on mask-rcnn," *Computers and Electronics in Agriculture*, vol. 163, p. 104846, 2019.
- [46] G. Cheng, J. Wang, K. Li, X. Xie, C. Lang, Y. Yao, and J. Han, "Anchor-free oriented proposal generator for object detection," *IEEE Transactions on Geoscience and Remote Sensing*, vol. 60, pp. 1–11, 2022.
- [47] Q. Lin, J. Zhao, G. Fu, and Z. Yuan, "Crpn-sfnet: A high-performance object detector on large-scale remote sensing images," *IEEE Transactions on Neural Networks and Learning Systems*, vol. 33, no. 1, pp. 416–429, 2020.

- [48] J. Redmon and A. Farhadi, "Yolov3: An incremental improvement," *arXiv preprint arXiv:1804.02767*, 2018.
- [49] A. Bochkovskiy, C.-Y. Wang, and H.-Y. M. Liao, "Yolov4: Optimal speed and accuracy of object detection," *arXiv preprint arXiv:2004.10934*, 2020.
- [50] C. Zhu, Y. He, and M. Savvides, "Feature selective anchor-free module for single-shot object detection," in *Proceedings of the IEEE/CVF conference on computer vision and pattern recognition*, 2019, pp. 840–849.
- [51] Q. Chen, Y. Wang, T. Yang, X. Zhang, J. Cheng, and J. Sun, "You only look one-level feature," in *Proceedings of the IEEE/CVF conference on computer vision and pattern recognition*, 2021, pp. 13 039–13 048.
- [52] K. Duan, S. Bai, L. Xie, H. Qi, Q. Huang, and Q. Tian, "Centernet: Keypoint triplets for object detection," in *Proceedings of the IEEE/CVF international conference on computer vision*, 2019, pp. 6569–6578.
- [53] P. Wang, P. Chen, Y. Yuan, D. Liu, Z. Huang, X. Hou, and G. Cottrell, "Understanding convolution for semantic segmentation," in *2018 IEEE winter conference on applications of computer vision (WACV)*. Ieee, 2018, pp. 1451–1460.
- [54] L.-C. Chen, G. Papandreou, I. Kokkinos, K. Murphy, and A. L. Yuille, "Deepplab: Semantic image segmentation with deep convolutional nets, atrous convolution, and fully connected crfs," *IEEE transactions on pattern analysis and machine intelligence*, vol. 40, no. 4, pp. 834–848, 2017.
- [55] S. Liu, D. Huang *et al.*, "Receptive field block net for accurate and fast object detection," in *Proceedings of the European conference on computer vision (ECCV)*, 2018, pp. 385–400.
- [56] Y. He, D. Xu, L. Wu, M. Jian, S. Xiang, and C. Pan, "Lffd: A light and fast face detector for edge devices," *arXiv preprint arXiv:1904.10633*, 2019.
- [57] L. Cui, P. Lv, X. Jiang, Z. Gao, B. Zhou, L. Zhang, L. Shao, and M. Xu, "Context-aware block net for small object detection," *IEEE Transactions on cybernetics*, vol. 52, no. 4, pp. 2300–2313, 2020.
- [58] W. Luo, Y. Li, R. Urtasun, and R. Zemel, "Understanding the effective receptive field in deep convolutional neural networks," *Advances in neural information processing systems*, vol. 29, 2016.
- [59] T.-Y. Lin, P. Dollár, R. Girshick, K. He, B. Hariharan, and S. Belongie, "Feature pyramid networks for object detection," in *Proceedings of the IEEE conference on computer vision and pattern recognition*, 2017, pp. 2117–2125.
- [60] L. Wang, L. Wang, Y. Zhu, A. Chu, and G. Wang, "Cdff: a fast and highly accurate method for recognizing traffic signs," *Neural Computing and Applications*, vol. 35, no. 1, pp. 643–662, 2023.
- [61] Q. Fu, J. Liu, X. Zhang, Y. Zhang, Y. Ou, R. Jiao, C. Li, and G. Mazzanti, "A small-sized defect detection method for overhead transmission lines based on convolutional neural networks," *IEEE Transactions on Instrumentation and Measurement*, 2023.
- [62] J. Zhang, Y. Lv, J. Tao, F. Huang, and J. Zhang, "A robust real-time anchor-free traffic sign detector with one-level feature," *IEEE Transactions on Emerging Topics in Computational Intelligence*, 2024.
- [63] J. Wang, Y. Chen, X. Ji, Z. Dong, M. Gao, and C. S. Lai, "Vehicle-mounted adaptive traffic sign detector for small-sized signs in multiple working conditions," *IEEE Transactions on Intelligent Transportation Systems*, 2023.
- [64] Z. Li, H. Chen, B. Biggio, Y. He, H. Cai, F. Roli, and L. Xie, "Toward effective traffic sign detection via two-stage fusion neural networks," *IEEE Transactions on Intelligent Transportation Systems*, 2024.



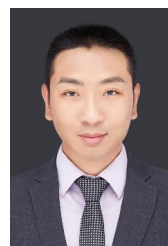
Heqiang Huang completed his B.Sc. in Electronic Information Science and Technology from Lanzhou University in 2023. He is presently pursuing his postgraduate studies in Transportation Engineering at the School of Intelligent Engineering, Sun Yat-sen University. Huang's research domain primarily revolves around computer vision, deep learning, and autonomous driving technologies.



Ronghui Zhang received a B.Sc. (Eng.) from the Department of Automation Science and Electrical Engineering, Hebei University, Baoding, China, in 2003, an M.S. degree in Vehicle Application Engineering from Jilin University, Changchun, China, in 2006, and a Ph.D. (Eng.) in Mechanical and Electrical Engineering from Changchun Institute of Optics, Fine Mechanics and Physics, the Chinese Academy of Sciences, Changchun, China, in 2009. After finishing his post-doctoral research work at INRIA, Paris, France, in February 2011, he is currently an Associate Professor with Guangdong Key Laboratory of Intelligent Transportation System, School of intelligent systems engineering, Sun Yat-sen University, Guangzhou, Guangdong 510275, P.R.China. His current research interests include computer vision, intelligent control and ITS.



Nengchao Lyu is a professor of Intelligent Transportation Systems Research Center, Wuhan University of Technology, China. He visited the University of Wisconsin-Madison as a visiting scholar in 2008. His research interests include advanced driver assistance system (ADAS) and intelligent vehicle (IV), traffic safety operation management, and traffic safety evaluation. He has hosted 4 National Nature Science Funds related to driving behavior and traffic safety; he has finished several basic research projects sponsored by the National Science and Technology Support Plan, Ministry of Transportation, etc. He has practical experience in safety evaluation, hosted over 10 highway safety evaluation projects. During his research career, he published more than 80 papers. He has won 4 technical invention awards of Hubei Province, Chinese Intelligent Transportation Association and Chinese Artificial Intelligence Institute.



Yanyong Guo received the M.S. degree in transportation engineering from Chang'an University, Xi'an, China, in 2012, and the Ph.D. degree in transportation engineering from Southeast University, Nanjing, China, in 2016. From 2014 to 2015, he was a Visiting Ph.D. Student with The University of British Columbia. He is currently a Professor with the School of Transportation, Southeast University. His research interests include road safety evaluations, traffic conflicts techniques, advanced statistical techniques for safety evaluation, and pedestrian and cyclist behaviors. He received the China National Scholarship, in 2014, and the Best Doctoral Dissertation Award from the China Intelligent Transportation Systems Association, in 2017.



Hong-Ning Dai is currently with the Department of Computer Science at Hong Kong Baptist University, Hong Kong as an associate professor. He obtained the Ph.D. degree in Computer Science and Engineering from Department of Computer Science and Engineering at the Chinese University of Hong Kong. His current research interests include the Internet of Things, big data, and blockchain technology. He has published more than 250 papers in top-tier journals and conferences with 19000+ citations. He has served as an associate editor for IEEE Communications Survey and Tutorials, IEEE Transactions on Intelligent Transportation Systems, IEEE Transactions on Industrial Informatics, IEEE Transactions on Industrial Cyber-Physical Systems, Ad Hoc Networks, and Connection Science. He is also a senior member of Association for Computing Machinery (ACM).



Junzhou Chen received his Ph.D. in Computer Science and Engineering from the Chinese University of Hong Kong in 2008, following his M.Eng degree in Software Engineering and B.S. in Computer Science & Applications from Sichuan University in 2005 and 2002, respectively. Between March 2009 and February 2019, he served as a Lecturer and later as an Associate Professor at the School of Information Science and Technology at Southwest Jiaotong University. He is currently an associate professor at the School of Intelligent Systems Engineering at Sun

Yat-sen University. His research interests include computer vision, machine learning, intelligent transportation systems, mobile computing and medical image processing.



Hong Yan received his PhD degree from Yale University. He was Professor of Imaging Science at the University of Sydney and currently is Wong Chun Hong Professor of Data Engineering and Chair Professor of Computer Engineering at City University of Hong Kong. Professor Yan's research interests include image processing, pattern recognition, and bioinformatics. He has over 600 journal and conference publications in these areas. Professor Yan is an IEEE Fellow and IAPR Fellow. He received the 2016 Norbert Wiener Award from the IEEE SMC Society

for contributions to image and biomolecular pattern recognition techniques. He is a member of the European Academy of Sciences and Arts and a Fellow of the US National Academy of Inventors.